

# Structure and Property of Interfaces in ARB Cu/Nb Laminated Composites

J. WANG,<sup>1,2</sup> K. KANG,<sup>1</sup> R. F. ZHANG,<sup>1</sup> S. J. ZHENG,<sup>1</sup> I. J. BEYERLEIN,<sup>1</sup>  
and N. A. MARA<sup>1</sup>

1.—Los Alamos National Laboratory, Los Alamos, NM 87545, USA. 2.—e-mail: wangj6@lanl.gov

Bulk Cu/Nb multilayered composites with high interfacial content have been synthesized via the accumulative roll bonding (ARB) method. Experimental characterization shows that these multilayers with submicrometer and nanometer individual layer thicknesses contain a predominant, steady-state interface with the Kurdjumov–Sachs orientation relationship joining the mutual {112} planes of Cu and Nb. In this article, we overview microscopy and simulation results on the structure of this interface at an atomic level and its influence on interface properties, such as interface shear resistance and its ability to absorb point defects and nucleate dislocations nucleation.

## INTRODUCTION

Grain boundaries and interphase interfaces in metals have been shown to play a fundamental role in material properties by acting as: (I) sources of defects, (II) sinks of defects via absorption and annihilation, (III) barriers to defects, and (IV) storage sites for defects.<sup>1–3</sup> Atomic-scale studies based on interface defect theory, atomistic simulations, and microscopy characterizations and measurements show that the atomic structure of an interface defines its properties and thereby the properties that they impart to polycrystalline and polyphasic materials.<sup>1–8</sup>

For metallic layered composites, most theoretical, modeling, and experiment studies find that material strength is related to interface type.<sup>3,4,9–13</sup> For coherent interfaces and semicoherent interfaces, coherency stresses play a crucial role in defining the maximum strength that can be achieved. For coherent interfaces in heterophases, the strength model<sup>14</sup> is based on the simple idea that a dislocation cannot traverse the composite unless the net forces on the dislocation in all layers are the same sign. Thus, a stress must be applied that at least cancels the coherency stress in one of the two constituents. For coherent interfaces in single-phase metals, the presence of twin boundaries causes the change of crystal orientations across the interface, resulting in the discontinuity of slip systems across twin boundaries, thereby strengthening

materials.<sup>15–19</sup> For semicoherent interfaces with small misfit, misfit dislocations relax only the long-range coherency stresses and the interface between the misfit dislocations remains coherent; therefore, a glide dislocation that intersects the coherent segment of interface in this region still encounters very large stresses.<sup>3,4,14</sup>

For interfaces between nonisostructural phases (such as between a face-centered cubic [fcc] and body-centered cubic [bcc] metal) with large misfit ( $> \approx 5\%$ ), atomic relaxations in the interface are complicated. However, geometric characters of interface planes determine the principal characteristics of interface structures. From the viewpoint of thermodynamics, interfaces composed of low-energy surfaces and/or low-energy ledges are energetically favorable, close to thermodynamic equilibrium. Two geometric factors are thus chosen to classify interfaces: compact plane and compact direction. In addition, the third factor is the similarity of the unit cell because it is likely to form a coherent structure for two crystallographic planes when their unit cells have similar atomic structures. With respect to the three geometric factors, we can classify the experimentally observed Cu/Nb incoherent interfaces with two different orientation relationships (Kurdjumov–Sachs [KS] and Nishiyama–Wassermann [NW]) into four types.<sup>20</sup> Type I: The interface consists of the compact planes of both crystals. Type II: The interface is not type I. That is, at least one of the two planes selected from each crystal for the interface is

noncompact for the respective crystal. The interface plane contains, however, the compact directions of the two crystals, and they are aligned. Type III: The interface is neither type I nor type II. The interface does not match the compact planes or the compact directions. The unit cells, however, are similar in that they have the same basic shape and the same number of atoms. Type IV: The interface does not belong to type I, type II, and type III.

The most commonly occurring incoherent fcc/bcc interfaces adopt KS or NW orientation relationships (OR).<sup>21–23</sup> When the two interface planes to be paired at the interface are compact, low-index planes, they tend to be atomically flat. Interfaces of this type tend to occur, for instance, in epitaxial growth (e.g., physical vapor deposition<sup>24,25</sup>) and examples include the KS or NW interfaces. The crystallographic planes joined at these interfaces, fcc {111} and bcc {110}, are atomically flat, corresponding to the type I interface. Consequently in equilibrium, the relaxed atomic structures of these interfaces are flat as well, free of steps and containing misfit dislocations with in-plane Burgers vectors.<sup>3,12</sup> Atomistic simulations show that the core of these misfit dislocations within these interfaces extends<sup>3,26</sup>, making it difficult for glide dislocation production via dissociation. As a consequence, lattice dislocation nucleation proceeds through an entirely different mechanism than observed previously for grain boundaries and stepped interfaces.<sup>27,28</sup> Also, such interfaces have a low shear resistance due to the easy creation and growth of interface dislocation loop at the intersection of these misfit dislocations.<sup>12</sup> In addition, Cu-Nb nanoscale multilayers fabricated by physical vapor deposition (PVD) can reach the superior radiation resistance due to core delocalization of two non-parallel misfit dislocations intersections.<sup>26</sup>

When two crystals are joined at crystallographic planes that are not atomically flat, the resulting relaxed equilibrium interface structure could either be disordered or ordered and faceted. Recently, Cu/Nb laminated composites have been synthesized through accumulative roll-bonding (ARB) method, and in submicrometers and nanometers contain a predominant, steady-state interface.<sup>29,30</sup> A five-parameter interface analysis<sup>30</sup> applied to all Cu-Nb interface pairs identifies most of the interfaces as  $\{112\}_{\text{fcc}}//\{112\}_{\text{bcc}}$  and  $\langle 111 \rangle_{\text{fcc}}//\langle 110 \rangle_{\text{bcc}}$ , or those close to it, which corresponds to the KS orientation relation. We abbreviate these interfaces as {112}KS or near-{112}KS and categorize them into type 2 interface in accordance with our classification. A recent study of ARB Cu/Nb layered composites at different scales on texture evolution, interface evolution, strength and ductility, and deformation mechanisms including slip transmission, dislocation nucleation, and deformation twinning, etc., shows that {112}KS interface is responsible for the phenomena observed in experiments.<sup>31–36</sup> The focus of this article is to overview recent investigations at atomic scale and to discuss an outlook for future work.

## INTERFACE STRUCTURES

Type II (or faceted) interfaces contain interfacial dislocations with Burgers vectors lying in-plane and out-of-plane of the interface and facets, where each facet or step is usually comprised of two faces (or terrace planes), which are described by its own crystallography. In this section, we present the method of characterizing the interface defects and optimizing the interface structure in terms of minimization of interface formation energy.

### Characterization of Interface Defects

For demonstration purposes, we choose an interface with a KS orientation relationship joining the mutual {112} planes of Cu and Nb that are observed in ARB Cu-Nb multilayers. A few methods for characterizing defect structure of interfaces are first reviewed.

#### *Frank–Bilby*

When two crystals are joined to form an interface, in general there exist some overlapping regions and/or gaps at the interface due to the incompatibilities and/or the dissimilarities between the two lattices. Accompanying the removal of the incompatibilities and/or the dissimilarities, interface defects or interface dislocations are required in the interface, which could act as stress annihilators to free the stresses far from the interfaces. Frank<sup>37</sup> and Bilby<sup>38</sup> provided a theory in which the net Burgers vector content  $\mathbf{B}(\vec{P})$  of the stress generators crossing a probe vector  $\vec{P}$  lying in the interface could be determined. As with most treatments of the problem, all of the detailed solutions are for the homogeneous, isotropic elastic approximation of coherency and defect fields. Considering an interface between bicrystals with lattices *A* and *B*, these lattices can be related to a common reference lattice by homogeneous distortion transformation matrices  $S_A$  and  $S_B$ . Let  $\vec{P}$  be a large vector in the interface where the vector must be large compared with any substructure within the interface, the net Burgers vector  $\mathbf{B}(\vec{P})$  crossing the interfacial vector  $\vec{P}$  can be calculated as  $\mathbf{B}(\vec{P}) = (S_A^{-1} - S_B^{-1})\vec{P}$ , where  $S_A^{-1}$  and  $S_B^{-1}$  are the inverse matrices of  $S_A$  and  $S_B$ . Driven by minimizing the chemical potential energy of interfaces, however, atoms within the interface in the two jointing crystals intend to match each other, forming coherent lattices within the interface. Therefore, a continuous distribution of interface Burgers content  $\mathbf{B}(\vec{P})$  will be energetically unfavorable and will prefer forming discrete interface dislocations.

#### *Geometry Model*

Interface defects can be characterized using a circuit mapping method,<sup>39–41</sup> which corresponds to a geometry description of Frank-Bilby equation. The Burgers vectors of the defects are defined with

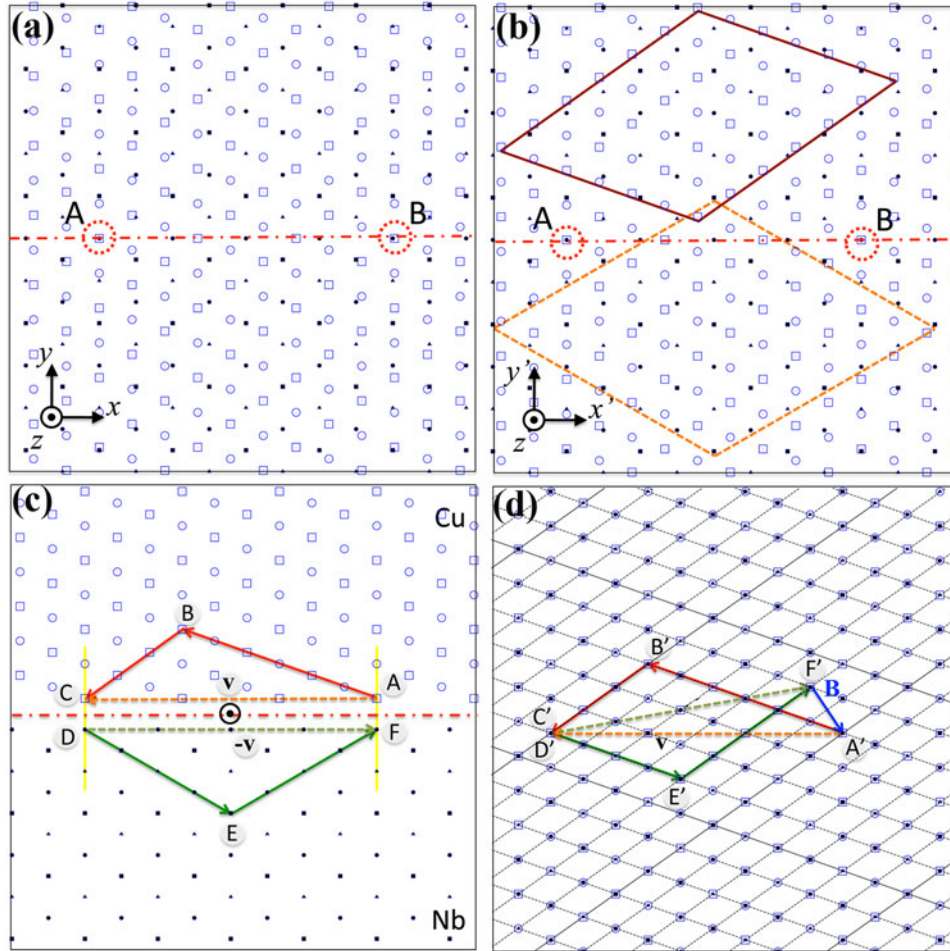


Fig. 1. Geometry model of the ideal-{112}KS interface in the bicrystal model. (a) Natural dichromatic pattern of Cu and Nb lattices with the parallel compact directions,  $(\bar{1}10)_{\text{fcc}} \parallel (1\bar{1}\bar{1})_{\text{bcc}}$ . Empty symbols designate Cu atoms and solid symbols designate Nb atoms. (b) Strained natural dichromatic pattern with imposed strains in (a). Cu and Nb lattices are relatively stretched in  $x$ -direction to match atoms at site A and B at the same time. (c) and (d) Illustrate the method of determining net Burgers content at an interface. A closed circuit in a bicrystal in (c) is created from the CDP (in b), and then the closed circuit in (c) is mapped in a coherent dichromatic pattern (CDP) (in d). The closure failure  $F'A'$  in (d) is the net Burgers vector  $[2.08 - 2.95]$  (Å) in the  $x$ - $y$  coordinate.

respect to a reference lattice, which is chosen as the coherent structure of the bimetal interface.<sup>40</sup> As a first step, we define the coherent dichromatic pattern (CDP) corresponding to this coherent structure. For the {112}KS interface, overlaying the projection of Cu and Nb crystals along the compact direction  $[1\bar{1}0]$  for Cu and  $1\bar{1}\bar{1}$  for Nb creates the natural dichromatic pattern shown in Fig. 1a. Along the  $x$ -axis, the two sets of lattice sites, marked by A and B, approximately, but not exactly overlap. To construct a coherent structure and make A and B coincide, one can deform both Cu and Nb by different amounts or deform one to match the other. In this example, we impose the extra strains separately to Cu and Nb while satisfying the equilibrium for a semi-infinite bilayer. The deformed crystals form the dichromatic pattern shown in Fig. 1b. Then, the dotted-line parallelogram in Fig. 1a can be mapped to the solid-line parallelogram in Fig. 1b. In the circuit mapping method, the reference

structure can be either one of the crystals or a mediated structure.<sup>41,42</sup> In our analysis, the Nb crystal is chosen to be the reference structure. We map both deformed crystals to the reference structure, forming the coherent dichromatic pattern (CDP) in Fig. 1d. A closed circuit is selected in the natural dichromatic pattern (real Cu-Nb bicrystal) in Fig. 1c and then mapped in the CDP. The closure failure corresponds to the net Burgers vector content, as shown in Fig. 1d.

### Disregistry

Atomistic simulations with reliable empirical potentials offer a powerful capability of characterizing atomic structures of an interface. For a relaxed interface, the disregistry analysis and/or the relative displacement analysis of the relaxed structure with respect to the unrelaxed structure can provide insights into understanding the relaxation



processes.<sup>43,44</sup> The applications of the two methods described above yield the net Burgers content  $\mathbf{B}(\bar{P})$  over a periodic length for a given interface. However, the net  $\mathbf{B}(\bar{P})$  is not sufficient for understanding the defect structure of an interface. It is desirable to know the position and Burgers vectors of the individual interface dislocations and the orientation relationships and lengths of the facets. Analyzing the relative displacements and disregistry of an atomic interface structure can provide the more resolved information.<sup>10–12</sup>

### Interface Defects of {112}KS Interface

Using molecular statics/dynamics simulations, we studied interface structures of three fcc/bcc systems, Cu-Nb, Al-Fe, and Al-Nb, and we found that the number of distinct sets of intrinsic interfacial dislocations and their core structures vary significantly among these three systems.<sup>33</sup>

For the Cu-Nb system, in which the lattice mismatch is 0.2469 along the  $x$ -axis and 0.3024 along the  $z$ -axis, the relaxed equilibrium structure of the {112}KS interface contains three sets of intrinsic dislocations. Figure 2a and b show the simulation model and the unrelaxed atomic structure in the  $x$ - $y$  plane. Figure 2c and d show the relaxed equilibrium structures in the  $x$ - $z$  plane and in the  $x$ - $z$  plane. Figure 2e shows atomic structure of interface defects. The line senses of sets 1 and 2 interface dislocations are oriented parallel to  $z$  and labeled with  $\mathbf{b}_1$  and  $\mathbf{b}_2$ , while the third set is oriented parallel to  $x$  and labeled as  $\mathbf{b}_3$ . Set 1 has its Burgers vector directed out of the interface plane, while sets 2 and 3 are misfit dislocations with in-plane Burgers vectors. As a result of the reaction of interface dislocations, the Cu-Nb interface holds three types of interface structures, in Fig. 2f, type 1 corresponds to the interface dislocations that are fully pinned, type 2 the interface dislocations that are partially pinned, and type 3 the interface dislocations that are fully depinned. Using the geometry model shown in Fig. 1d, the closed circuit A-B-C-D-E-F-A is chosen to enclose one periodic length (corresponding to the periodicity of the BUC) along the  $[111]\text{Cu}/[110]\text{Nb}$ . This length is obtained from MD simulations to be 18.7477 (Å).<sup>33</sup> The circuit is right-handed with the line direction of the encircled interface dislocation pointing out of the paper. The closure failure  $F'A'$  is found to be [2.08–2.95] (Å) in the  $x$ - $y$  coordinate, which corresponds to the net Burgers vector  $\mathbf{B}(\bar{P})$  in the  $x$ - $y$  coordinate. For a molecular dynamics (MD)-derived atomic structure of the Cu-Nb {112}KS interface, disregistry analysis are plotted in Fig. 2g, the  $x$  component  $b_x = 2.08$  Å agrees with both  $F'A'$  in Fig. 1d and  $\mathbf{B}(\bar{P})$  from the F-B equation.<sup>33</sup> Moreover, the pure edge misfit dislocation (i.e., with its  $y$ -component = -2.95 Å) has dissociated into Shockley partials that extend into Cu, normal to the interface. The Burgers vector of these partials is 1.47 Å and thus the rest of the  $y$

component, which is -1.48 Å, remains at the interface. The disregistry analysis along the  $z$ -axis shows that set 3 interface dislocation  $\mathbf{b}_3$  has the Burgers vector of  $a_{\text{Cu}}[\bar{1}10]/2$  and is separated by the average spacing of 24.8 Å.

For the Al-Fe interface, all three sets of interfacial dislocations remain in the interface and have not dissociated into Al, as a result of the high stacking fault energy (SFE) of Al. The set 1 dislocations  $\mathbf{b}_1 = [0.0 \ 2.3\text{--}2.5 \ 0.0]$  Å remain in the plane of the interface, unlike in the Cu-Nb interface, where the Shockley partials are seen to extend from the interface as a result of a dissociation of the  $\mathbf{b}_1$  intrinsic dislocation. The average spacing of the set 1 dislocation is 25.6 Å. Compared to the Cu-Nb interface, these spacings are larger due to differences in the faceted topology of the Al and Fe {112} planes. The misfit set 2 dislocations are edge dislocations with the Burgers vector  $\mathbf{b}_2 = a_{\text{Al}}[111]/3$ . They are spaced along  $x$  about 15.4 Å, which is finer than that for the set 2 dislocations in Cu-Nb, due to the greater mismatch in Al-Fe than Cu-Nb. The misfit set 3 dislocations could have the Burgers vector  $\mathbf{b}_3 = a_{\text{Al}}[\bar{1}10]/2$  if the spacing is chosen to be 18.5 (Å). However, it is not well defined from atomic structures due to its core spreading within the interface plane along the  $z$ -axis. Compared with the core structure of the set 3 dislocations in Cu-Nb, the core of a set 3 dislocation at the interaction with  $\mathbf{b}_1$  has not dissociated into the nonplanar structure due to the higher SFE in Al than Cu. In Al-Fe, the set 3 dislocations can spread in-plane since forming a fault in the interface has a lower energy penalty than forming a stacking fault in Al. The opposite is true for Cu-Nb. Set 3 has a compact core in Cu-Nb, with the exception of the intersection points with set 1, where it dissociates into the Cu crystal onto two {111} planes.

In the extreme case that the lattice mismatch is negligible, the {112}KS interface would only contain the set 1 interfacial dislocations. The Al-Nb {112}KS interface provides one such example, with a lattice mismatch of 0.0037 (Å) in the  $x$ -direction and 0.0045 (Å) in the  $z$ -direction, substantially lower than those of Cu-Nb and Al-Fe. Only the set 1  $\mathbf{b}_1 = [0.0 \ 2.14 \ 0.0]$  (Å) dislocations can be identified with its spacing of 14.0 Å. Obviously like the Al-Fe system, the set 1 dislocations in the Al-Nb system do not extend into Al and remain in the plane of the interface. Sets 2 and 3 are not present since the in-plane lattice mismatches in both  $x$  and  $z$  are negligible for this fcc/bcc system.

In summary, atomistic simulations reveal that the interface contains at least one and at most three sets of intrinsic interface dislocations. At minimum, one set with the Burgers vector lying out of the interface plane is needed to accommodate differences in the faceted nature of the surfaces of the {112} planes. At most, two more sets with Burgers vectors lying within the interface plane are required to accommodate the lattice mismatch parallel to the interface plane.

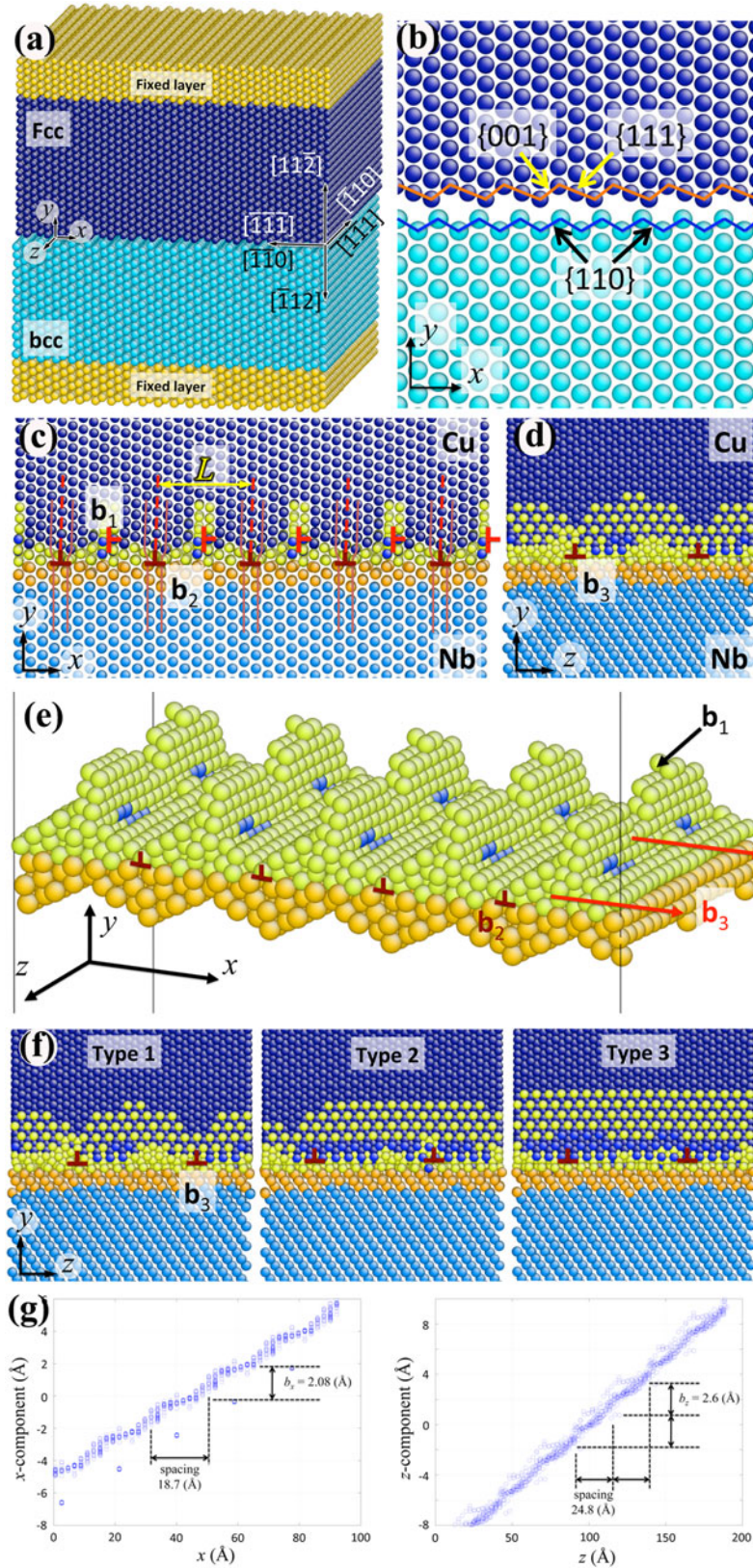


Fig. 2. (a) Simulation model, (b) the unrelaxed interface structure, (c) the relaxed interface structure in the  $x$ - $y$  plane, (d) in the  $y$ - $z$  plane, and (e) interface defect structure in the  $x$ - $y$ - $z$  coordinate. (f) Three types of interfaces with respect to the reaction between set 1 and set 3 interface dislocations. (g) Disregistry analysis showing the spacings and Burgers vectors at the Cu/Nb interface.



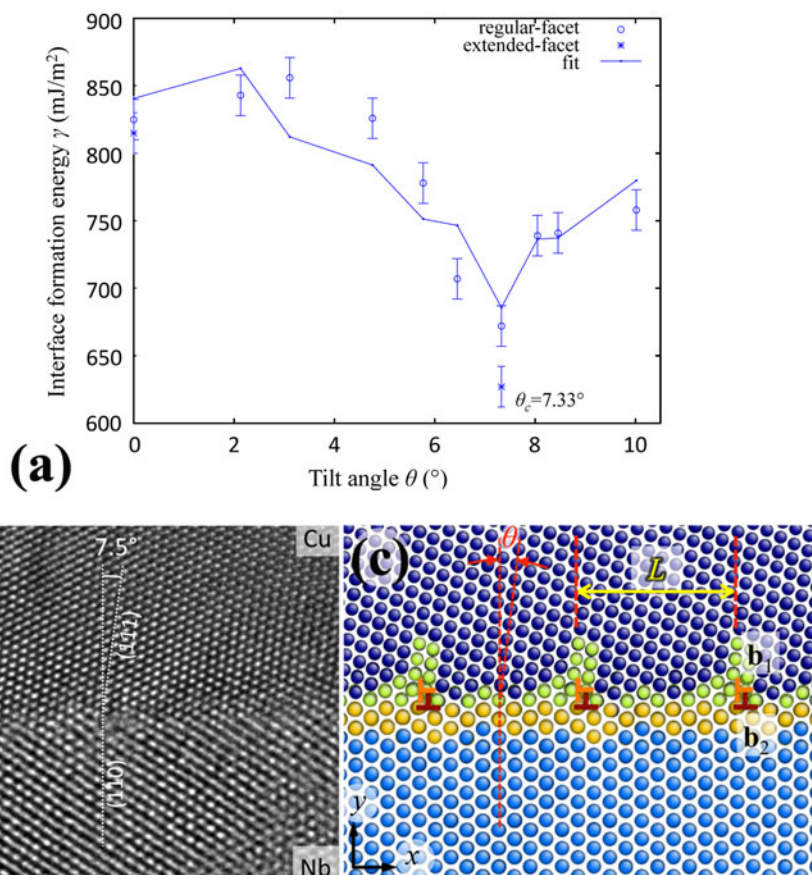


Fig. 3. Minimization of interface formation energy in association with the deviation of misorientation from the ideal  $\{112\}$ KS interface. (a) Interface formation energy. Atomic structure of the interface with a deviation of  $7.33^\circ$ , (b) TEM image, and (c) atomistic simulation.

### Interface Optimization

Due to the presence of the set 1 dislocations that have an out-of-plane Burgers vector, the  $\{112\}$ KS OR might be destroyed by nucleation and emission of a lattice dislocation from the interface, driven by reducing the Burgers vector content in the interface.<sup>42</sup> Therefore, “near- $\{112\}$ KS interfaces” might have the low formation energy and be more thermally stable. Texture analysis<sup>29,45</sup> shows that such deviation could be due to a tilt and/or twist of either or both crystals with respect to the ideal  $\{112\}$ KS interface. As a first step in understanding its origin, we consider deviations created by tilting one of the crystals about the parallel compact directions  $\langle 110 \rangle_{\text{fcc}} // \langle 111 \rangle_{\text{bcc}}$ .

For near- $\{112\}$ KS interfaces, the Cu crystal is tilted clockwise about the  $z$ -axis with respect to the ideal  $\{112\}$  KS interface at nine discrete angles  $\theta$ :  $2.13^\circ$ ,  $3.11^\circ$ ,  $4.76^\circ$ ,  $5.77^\circ$ ,  $6.45^\circ$ ,  $7.33^\circ$ ,  $8.05^\circ$ ,  $8.46^\circ$ , and  $10.02^\circ$ , while keeping Nb fixed. Corresponding to  $\theta$ , the Cu orientation normal to the  $\{112\}$  interface plane of Nb is  $[66\bar{1}3]$ ,  $[44\bar{9}]$ ,  $[55\bar{1}2]$ ,  $[22\bar{5}]$ ,  $[77\bar{1}8]$ ,  $[33\bar{8}]$ ,  $44\bar{1}1$ ,  $55\bar{1}4$ , and  $[11\bar{3}]$ , respectively. Atomistic simulations are performed along the periodic boundary condition along the  $x$ - and  $z$ -axis, while the fixed boundary condition is applied along

the  $y$ -axis.<sup>33</sup> In all cases of  $\theta$  from  $0^\circ$  to  $11^\circ$ , the interface planes being joined are not compact; atoms follow a serrated path with alternating  $\{001\}$  and  $\{111\}$  planes on the Cu side and alternating non-parallel  $\{110\}$  planes on the Nb side. Figure 3a shows the interface formation energy  $\gamma$  as a function of tilt angle  $\theta$ . It is found that  $\gamma$  reduces substantially to a minimum of  $\gamma = 672 \text{ (mJ/m}^2\text{)}$  at  $\theta = 7.33^\circ$ , and the Burgers vector content in this interface is equal to  $[1.97\ -1.0]$  (Å) in the  $x$ - $y$  coordinate, which is smaller than  $[2.08\text{--}2.95]$  (Å) in the  $\{112\}$ KS interface, in particular, the out-of-interface component decreases from 2.95 to 1.0 (Å). Interestingly, interfaces with approximately the same tilt angle are directly observed and measured from transmission electron microscopy (TEM) image within an ARB sample, as shown in Fig. 3b and c.

## INTERFACE PROPERTIES

### Point Defects

Accompanying with the formation of dislocation jogs within interface, an interface can act as sinks or sources of point defects and the ability to absorb point defects depends on the atomic structure of the dislocation intersections.<sup>26,33</sup> Using atomistic

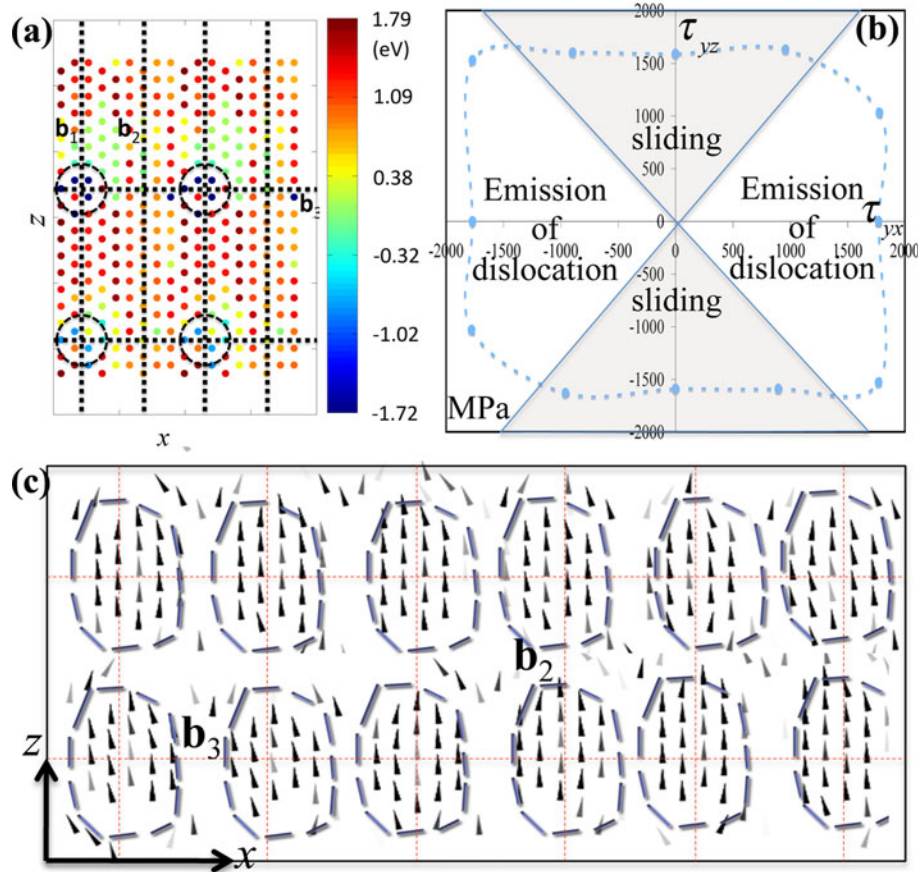


Fig. 4. Interface properties. (a) VFE maps for Cu-Nb. VFE is negative around the circled regions, where  $b_1$  and  $b_3$  are pinned at the intersection. (b) The two-dimensional flow strength of  $\{112\}$ KS interface. (c) Interface sliding mechanism as the interface is sheared along the z-axis.

simulations, for the Cu-Nb and Al-Fe interfaces, we found that the intersections of interface dislocations act as favorable sites for vacancy absorption. However, the Al-Nb interface, with no intersection points, contains no sites for vacancy absorption, and thus, it is the worst structure studied here for vacancy absorption. To calculate the vacancy formation energies (VFEs) at a given point in the interface, an fcc atom is removed from the regions around the intersections of interface dislocations and the defected interface is then relaxed using the conjugate gradient algorithm. The resulting VFE maps for the Cu-Nb material systems are shown in Fig. 4a. Overall, we find that the VFEs are the lower along the intrinsic dislocation lines than outside of them and the lowest at the intersection points.

In the Cu-Nb interface, the VFE is negative locally at and near the intersection region between set 1 and set 3 (Fig. 4a). These points correspond to the points where the set 1 dislocation is pinned to the interface. At the intersection between set 2 and set 3, the two in-plane edge dislocations, the VFE is positive but still lower than bulk Cu VFE. It is worth pointing out that interface will change the structure from type 1 to type 2 to type 3 accompanying with the absorption of vacancy at the

intersection region between set 1 and set 3 dislocations. In type 3, the VFE is positive everywhere, although it is still much lower than the VFE in bulk Cu 1.299 (eV). Compared to the Cu-Nb interface, the Al-Fe and Al-Nb interfaces, represent two opposite extremes in their ability to absorb vacancies. In the Al-Fe interface, the interfacial regions of VFE lower than bulk VFE (0.685 eV) are not localized, which is a consequence of the extended core of the set 3 dislocations. Its defect structure consists of an intersecting network of intrinsic dislocations whose cores are spread within the interface. As shown here, this structure results in significantly large regions of VFE lower than bulk VFE (0.685 eV) and, thus, an interface that would be an excellent sink for vacancies. In contrast, in the Al-Nb interface, the VFE is positive everywhere and higher than bulk VFE (0.733 eV) almost everywhere. Only in the neighborhood of the set 1 dislocations, the VFE is slightly lower than that of bulk Al (0.733 eV). The Al-Nb interface is a poor sink for vacancies for two reasons. First, because the Al-Nb interface only contains one set of parallel dislocations and hence no intersection points, it lacks regions where the VFE is negative. Second, the cores of the interfacial dislocations belonging to this array are compact.

## Shear Response

Shear response of interface has been studied by using atomistic simulation with a bilayer model.<sup>10–12</sup> A gradually increasing shear strain is applied homogeneously to bilayer models of Cu-Nb along the different shear directions while maintaining equilibrium, i.e.,  $\sigma_{yx}^{\text{Cu}} = \sigma_{yx}^{\text{Nb}}$  and  $\sigma_{yz}^{\text{Cu}} = \sigma_{yz}^{\text{Nb}}$ . The shear stresses  $\sigma_{yx}$  and  $\sigma_{yz}$  parallel to the interface are generated by applying the displacement gradients,  $\partial u/\partial y$  and  $\partial w/\partial y$ , to the two crystals.  $u$  and  $w$  are the displacements along  $x$  and  $z$  directions. Shearing of the two crystals is achieved by maintaining their ratio constant at every loading step. Because of the difference in shear moduli, the ratio of displacement gradients  $\partial u/\partial y$  and  $\partial w/\partial y$  to maintain equilibrium in the Nb crystal differs from that in Cu, and the increments of displacement gradients differ. The boundary conditions in the models were satisfied while departures from equilibrium were minimized by incrementing the displacement gradients such that the shear stress increments were less than 30 MPa at each loading step. The tolerance of 30 MPa is chosen to prevent overshooting shear strength of interface when applying shear strain increments. After applying the displacement gradient increments to the two crystals, all atomic positions are then allowed to relax fully and independently. During shearing of the two crystals, disregistry analysis was employed to determine slip in interface. Figure 4b shows the two-dimensional flow stresses with respect to the shear direction. The flow stresses is determined corresponding to the occurrence of the irreversible sliding within interface or the nucleation and emission of lattice dislocation from interface. With respect to the shear directions in the range of  $\pm 40^\circ$  around the compact direction, shear resistance varies with the angle, but the projection on the compact direction is approximately constant at 1.5 GPa. Figure 4c shows the result of disregistry analysis with respect to the shear direction along the compact direction, implying that the interface shear is accomplished through the creation and subsequent growth of interface dislocation loops that initialize at the intersection region between set 1 and set 3 dislocations, similar with interface shear mechanisms in atomic flat PVD KS and NW interfaces.<sup>12</sup> For the other shear directions, interface does not undergo the shear displacements. Instead, interface dislocation  $\mathbf{b}_3$  moves either extending or shrinking the stacking faults with respect to the shear stress, which is a generic response for interface that contains the out-of-plane Burgers vector.<sup>43</sup>

## Dislocation Nucleation

Besides the nucleation of interfacial glide dislocation loop within interface, lattice dislocations will nucleate at interface and glide into the adjoining crystals under mechanical loading.<sup>27,28</sup> The Schmid factor analysis associated with each Cu Shockley

partial dislocations on the four {111} planes (in Fig. 5a) indicates multiple slip systems that can be activated under a given stress. However, atomistic simulations revealed that the selected slip systems do not necessary follow the Schmid factor analysis, as shown in Fig. 5b and c.

During MD simulations, the bilayer model was uniformly strained in increments of 0.2%. At each increment, the strained system was relaxed until the uniaxial stress condition is satisfied, and then we apply dynamic quenching MD until the maximum residual force on each atom becomes less than 5 pN. When stretching the bilayer model along the  $x$ -axis, the partial  $b_1$  on  $(\bar{1}\bar{1}1)$  is activated, but the other two partials  $b_1$  on  $(\bar{1}1\bar{1})$  and  $b_1$  on  $(1\bar{1}\bar{1})$  are not activated although the three partials have the maximum Schmid factor of 0.314. The nucleation site is located at the line of the set 2 interface dislocations, and the line of the freshly nucleated partial shares the trace of the activated glide plane  $(\bar{1}\bar{1}1)$  on the interface. The relative displacement analysis was performed in the core region of set 2 dislocation, indicating that the set 2 dislocation has the nonplanar core structure, i.e., the core spreads on the  $(111)$  plane (in Fig. 5d) and facilitates the nucleation and emission of a partial  $b_1$  on  $(\bar{1}\bar{1}1)$ . In comparison, when stretching the bilayer model along the  $z$ -axis or the  $y$ -axis, the partial  $b_3$  are activated on either  $(\bar{1}\bar{1}\bar{1})$  or  $(1\bar{1}\bar{1})$  plane but the other partials  $b_1$  and  $b_2$  on the two planes are not activated although the Schmid factor is positive. The more important result is that the nucleation takes place at the intersection of interface dislocations set 1 and set 3. It should be mentioned that set 3 interface dislocation has a Burgers vector of  $\frac{a}{2} [110]$  and its line sense along  $[111]$ , corresponding to a pure edge dislocation on the interface plane. Relative displacement analysis in the core region indicates the non-planar core structure, dissociates on the two planes  $(\bar{1}\bar{1}\bar{1})$  and  $(1\bar{1}\bar{1})$ , as indicated in Fig. 5d. The disregistry analysis on the two planes show that the shear displacement on the two plane is along  $b_2$  on  $(\bar{1}\bar{1}\bar{1})$  and  $(1\bar{1}\bar{1})$ . As a consequence, the nonplanar core structure facilitates the nucleation and emission of the two partials with the resolved shear stresses being positive on these two slip systems. Besides the three glide planes, partial dislocation  $b_1$  can nucleate and glide on the fourth plane  $(111)$ , which corresponds to set 1 interface dislocation. As we discussed above, set 1 interface dislocation takes part of the Burgers vector content within the interface; thus, the nucleation of set 1 interface dislocation can be considered as the dissociation of intrinsic interface dislocation content.

MD simulations combined with analysis of the core structure of interface dislocations reveal the mechanisms of nucleation of lattice dislocation from a faceted interface. When interface dislocation lines do not lie on the glide plane of the activated slip system, the nucleation will initialize at the intersection of two sets of interface dislocations, and the



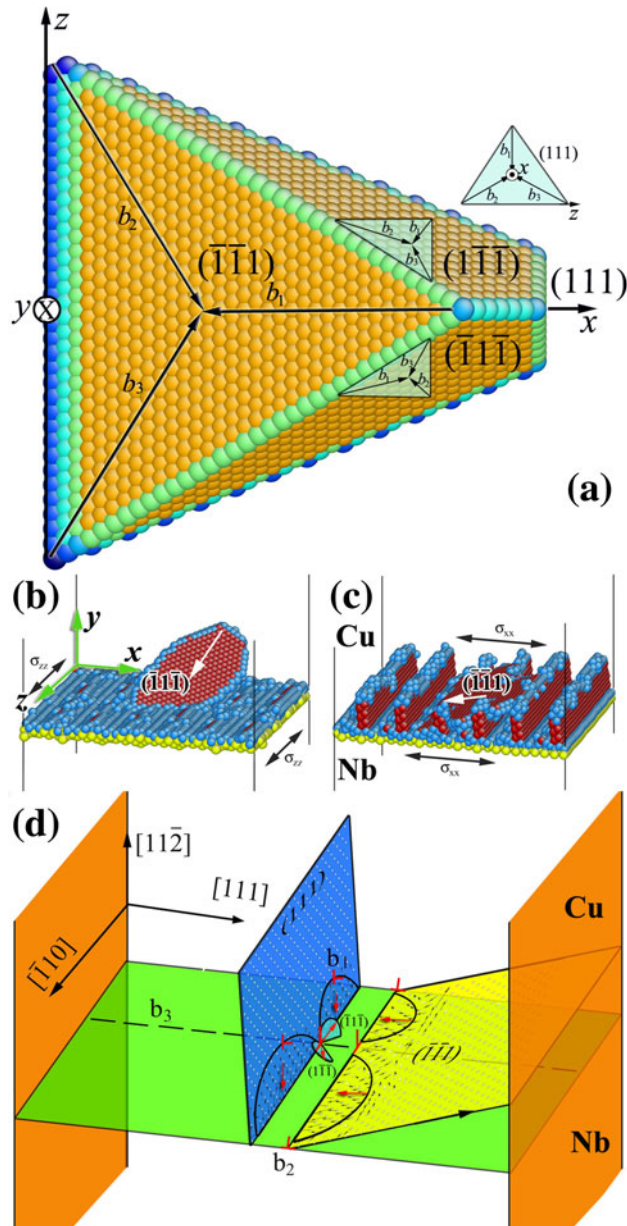


Fig. 5. Dislocation nucleation at  $\{112\}$ KS interface. (a) Slip systems in Cu. Atomic simulations show the nucleation of partial dislocations from interface as (b) stretching along the  $x$ -axis and (c) stretching along the  $z$ -axis. (d) The correlation of partials with the core structure of interface dislocations.

character of the nonplanar core of interface dislocation determines the selected slip system. When the interface dislocation line lies on the glide plane of the activated slip system, nucleation will initiate at the interface dislocation segment that lies between other interface dislocations, and the character of the nonplanar core of the interface dislocation determines the selected slip system. Thus, the activated slip system is correlated with the microstructure and the core structure of the interface dislocations.

## SUMMARY

Based on characterization by high-resolution transmission electron microscopy and atomistic simulations, current work on multilayers revealed that type II interfaces contains at least one and at most three sets of intrinsic interface dislocations. At minimum, one set with the Burgers vector lying out of the interface plane is needed to accommodate differences in the faceted nature of the crystallographic surfaces. At most, two more sets with Burgers vectors lying within the interface plane are required to accommodate the lattice mismatch parallel to the interface plane. As a consequence, the atomic structure of the interface leads to specific properties of the interface, as follows:

1. The sink ability to absorb point defects is related to the intersection of interface dislocations
2. Interface shear is accomplished either through interface sliding along the compact direction or emission of lattice dislocation that nucleates in association with the nonplanar core structure of interface dislocation
3. Dislocation nucleation is correlated to the microstructure and core structure of intrinsic dislocations.

In addition to atomic-scale study, other methods such as discrete dislocation dynamics and crystal plasticity modeling are being used, and this will lead to multiscale models that predict the complete stress-strain curve and texture evolution using atomic-scale deformation mechanisms at interfaces. The field of research in metallic multilayers continues to grow with exploration of other properties such as fatigue and fracture, creep, and shock.

## ACKNOWLEDGEMENTS

This work was supported by the Center for Materials at Irradiation and Mechanical Extremes, an Energy Frontier Research Center funded by the U.S. Department of Energy, Office of Science, Office of Basic Energy Sciences under award number 2008LANL1026. For the defect characterization method development, J.W. acknowledges support provided by the Los Alamos National Laboratory Directed Research and Development (LDRD) projects DR20110029 and ER20110573.

## REFERENCES

1. A.P. Sutton and R.W. Balluffi, *Interfaces in Crystalline Materials* (New York: Oxford University Press, 1997).
2. J.P. Hirth, *Metall. Trans.* 3, 3047 (1972).
3. M.J. Demkowicz, J. Wang, R.G. Hoagland, *Dislocations in Solids*, vol. 14, Chapter 83 (Amsterdam: Elsevier North-Holland, 2008), p. 143.
4. J. Wang and A. Misra, *Curr. Opin. Solid State Mater. Sci.* 15, 20 (2011).
5. C.N. Tomé, I.J. Beyerlein, J. Wang, and R.J. McCabe, *JOM* 63, 19 (2011).
6. J. Wang, I.J. Beyerlein, and C.N. Tomé, *Scripta Mater.* 63, 741 (2010).

7. J. Wang and I.J. Beyerlein, *Modell. Simul. Mater. Sci. Eng.* 20, 024002 (2012).
8. J. Wang, I.J. Beyerlein, and J.P. Hirth, *Modell. Simul. Mater. Sci. Eng.* 20, 024001 (2012).
9. J. Wang, A. Misra, R.G. Hoagland, and J.P. Hirth, *Acta Mater.* 60, 1503 (2012).
10. J. Wang, R.G. Hoagland, X.Y. Liu, and A. Misra, *Acta Mater.* 59, 3164 (2011).
11. J. Wang, R.G. Hoagland, J.P. Hirth, and A. Misra, *Acta Mater.* 56, 5685 (2008).
12. J. Wang, R.G. Hoagland, J.P. Hirth, and A. Misra, *Acta Mater.* 56, 3109 (2008).
13. N. Li, N. Mara, J. Wang, P. Dickerson, J.Y. Huang, and A. Misra, *Scripta Mater.* 67, 479 (2012).
14. R.G. Hoagland, T.E. Mitchell, J.P. Hirth, and H. Kung, *Philos. Mag.* 82, 643 (2002).
15. L. Lu, X. Chen, X. Huang, and K. Lu, *Science* 323, 607 (2009).
16. K.A. Afanasyev and F. Sansoz, *Nano Lett.* 7, 2056 (2007).
17. J. Wang and H. Huang, *Appl. Phys. Lett.* 88, 203112 (2006).
18. N. Li, J. Wang, X. Zhang, and A. Misra, *JOM* 63, 63 (2011).
19. N. Li, J. Wang, A. Misra, X. Zhang, J.Y. Huang, and J.P. Hirth, *Acta Mater.* 59, 5989 (2011).
20. J. Wang, I.J. Beyerlein, A. Misra, S.M. Valone, and T.C. Germann, *Advances in Heterogeneous Material Mechanics*, ed. J. Fan, J. Zhang, H. Chen, and Z.H. Jin (Lancaster, PA: DEStech Publications, Inc., 2011), p. 39–46.
21. B.M. Clemens, H. Kung, and S.A. Barnett, *MRS Bull.* 24, 20 (1999).
22. A. Misra and H. Kung, *Adv. Eng. Mater.* 3, 217 (2001).
23. A. Misra, M.J. Demkowicz, J. Wang, and R.G. Hoagland, *JOM* 60, 39 (2008).
24. N.A. Mara, D. Bhattacharyya, A. Misra, and R.G. Hoagland, *Scripta Mater.* 58, 874 (2008).
25. N.A. Mara, D. Bhattacharyya, P. Dickerson, R.G. Hoagland, and A. Misra, *Appl. Phys. Lett.* 92, 231901 (2008).
26. M.J. Demkowicz, R.G. Hoagland, and J.P. Hirth, *Phys. Rev. Lett.* 100, 136102 (2008).
27. R.F. Zhang, J. Wang, I.J. Beyerlein, and T.C. Germann, *Scripta Mater.* 65, 1022 (2011).
28. R.F. Zhang, J. Wang, I.J. Beyerlein, A. Misra, and T.C. Germann, *Acta Mater.* 60, 2855 (2012).
29. J.S. Carpenter, S.C. Vogel, J.E. LeDonne, D.L. Hammon, I.J. Beyerlein, and N.A. Mara, *Acta Mater.* 60, 1576 (2012).
30. S.-B. Lee, J.E. LeDonne, S.C.V. Lim, I.J. Beyerlein, and A.D. Rollett, *Acta Mater.* 60, 1747 (2012).
31. S.J. Zheng, I.J. Beyerlein, J. Wang, J.S. Carpenter, W.Z. Han, and N.A. Mara, *Acta Mater.* (2012). doi: [10.1016/j.actamat.2012.07.027](https://doi.org/10.1016/j.actamat.2012.07.027).
32. W.Z. Han, J.S. Carpenter, J. Wang, I.J. Beyerlein, and N.A. Mara, *Appl. Phys. Lett.* 100, 011911 (2012).
33. K. Kang, J. Wang, and I.J. Beyerlein, *J. App. Phys.* 111, 053531 (2012).
34. N.Q. Vo, R.S. Averback, Y. Ashkenazy, P. Bellon, and J. Wang, *J. Mater. Res.* 27, 1621 (2012).
35. M.J. Demkowicz and L. Thilly, *Acta Mater.* 59, 7744 (2011).
36. R.F. Zhang, J. Wang, X.Y. Liu, I.J. Beyerlein, and T.C. Germann (Paper presented at the Shock Compression of Condensed Matter 2011, AIP Conference Proceedings 1426, 2011), pp. 1251–1254.
37. F.C. Frank, *Report of the symposium on the plastic deformation of crystalline solids* (Pittsburgh: Carnegie Institute of Technology, 1950), p. 150.
38. B.A. Bilby, *Report of the Conference on Defects in Crystalline Solids* (London: Physical Soc, 1955), p. 124.
39. R.C. Pond and J.P. Hirth, *Solid State Phys.* 47, 287 (1994).
40. R.C. Pond, X. Ma, Y.W. Chai, and J.P. Hirth, *Dislocations in Solids*, Chap. 74 (Elsevier, Amsterdam, 2007).
41. J.P. Hirth and R.C. Pond, *Prog. Mater. Sci.* 56, 586 (2011).
42. J. Wang, J.P. Hirth, R.C. Pond, and J.M. Howe, *Acta Mater.* 59, 241 (2011).
43. J. Wang, A. Misra, and J.P. Hirth, *Phys. Rev. B* 83, 064106 (2011).
44. J. Wang, J.P. Hirth, A. Misra, and X. Zhang, *Appl. Phys. Lett.* 95, 021908 (2009).
45. J.S. Carpenter, X. Liu, A. Darbal, N.T. Nuhfer, R.J. McCabe, and S.C. Vogel, et al., *Scripta Mater.* 67, 336 (2012).